Healthy and diseased coronary bifurcation geometries influence near-wall and intravascular flow: A computational exploration of the hemodynamic risk

Claudio Chiastra [a,b,1], Diego Gallo [c,1], Paola Tasso [c], Francesco Iannaccone [d], Francesco Migliavacca [b], Jolanda J. Wentzel [a], Umberto Morbiducci [c,*]

[a] Department of Cardiology, Biomedical Engineering, Erasmus MC, Rotterdam, The Netherlands
[b] Laboratory of Biological Structure Mechanics (LaBS), Department of Chemistry, Materials and Chemical Engineering "Giulio Natta", Politecnico di Milano, Milan, Italy
[c] Polito[BIO]Med Lab, Department of Mechanical and Aerospace Engineering, Politecnico di Torino, Turin, Italy
[d] FEops NV, Ghent, Belgium

Local hemodynamics has been identified as one main determinant in the onset and progression of atherosclerotic lesions at coronary bifurcations. Starting from the observation that atherosensitive hemodynamic conditions in arterial bifurcation are majorly determined by the underlying anatomy, the aim of the present study is to investigate how peculiar coronary bifurcation anatomical features influ-ence near-wall and intravascular flow patterns. Different bifurcation angles and cardiac curvatures were varied in population-based, idealized models of both stenosed and unstenosed bifurcations, representing the left anterior descending (LAD) coronary artery with its diagonal branch. Local hemodynamics was analyzed in terms of helical flow and exposure to low/oscillatory shear stress by performing computa-tional fluid dynamics simulations.

Results show that bifurcation angle impacts lowly hemodynamics in both stenosed and unstenosed cases. Instead, curvature radius influences the generation and transport of helical flow structures, with smaller cardiac curvature radius associated to higher helicity intensity. Stenosed bifurcation models exhibit helicity intensity values one order of magnitude higher than the corresponding unstenosed cases. Cardiac curvature radius moderately affects near-wall hemodynamics of the stenosed cases, with smaller curvature radius leading to higher exposure to low shear stress and lower exposure to oscillatory shear stress. In conclusion, the proposed controlled benchmark allows investigating the effect of various geometrical features on local hemodynamics at the LAD/diagonal bifurcation, highlighting that cardiac cur-vature influences near wall and intravascular hemodynamics, while bifurcation angle has a minor effect.

Keywords: Atherosclerosis, Hemodynamic hypothesis, Wall shear stress, Helical flow, Coronary bifurcation, Computational fluid dynamics

1. Introduction

Atherosclerosis is a chronic inflammatory disease of the arterial wall that progressively reduces the lumen size because of plaque formation. It is widely recognized that atherosclerotic lesions develop at preferential anatomic locations such as coronary bifurcations (Antoniadis et al., 2015), accounting for 15–20% of the lesions present in the coronary arteries (Lassen et al., 2016).

The so-called "hemodynamic hypothesis" suggests that local hemodynamics is a main factor of the onset and progression of lesions at coronary bifurcations (Morbiducci et al., 2016). In particular, low and oscillatory wall shear stress (WSS) phenotypes have been identified as a key factor in plaque formation and progression (Kwak et al., 2014).

Local hemodynamics is mainly determined by the underlying anatomical features of an arterial bifurcation. In carotid arteries, computational fluid dynamics (CFD) studies have demonstrated a correlation between geometry and disturbed shear (Bijari et al., 2012; Lee et al., 2008). Accordingly, geometrical features showed to be associated with the presence of atherosclerotic plaques (Bijari et al., 2014; Morbiducci et al., 2016). Furthermore, local geometry of carotid bifurcation has been reported to be significantly correlated with peculiar intravascular flow features, in particular helical flow structures (Gallo et al., 2015), which in turn

* Corresponding author at: Department of Mechanical and Aerospace Engineering, Politecnico di Torino, Corso Duca degli Abruzzi 24, 10129 Turin, Italy.
E-mail address: umberto.morbiducci@polito.it (U. Morbiducci).
[1] C. Chiastra and D. Gallo contributed equally.

Article history:
Accepted 11 April 2017

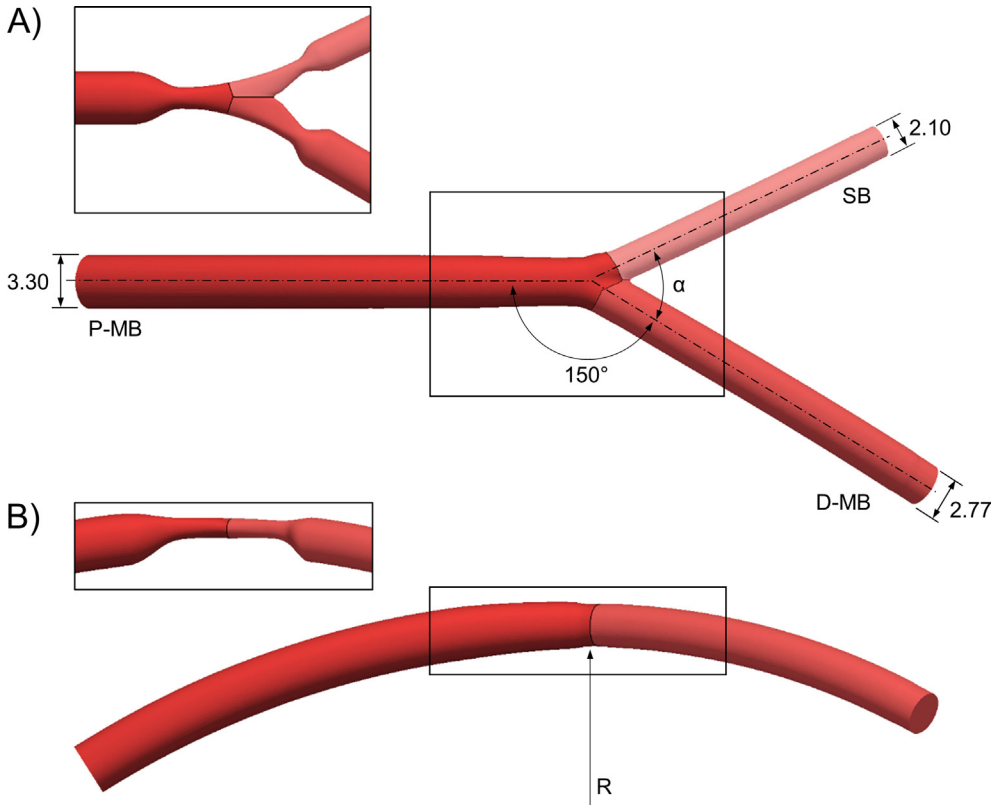

Fig. 1. Parametric model of the healthy left anterior descending – first diagonal coronary bifurcation: (A) top view; (B) lateral view. Details of the diseased model are shown in the boxes. Diameters are in millimeters. The different colors in the top view indicate the three regions, i.e. proximal main branch (P-MB), distal main branch (D-MB), and side branch (SB), in which the model was divided for the analyses of the near-wall and bulk flow quantities.

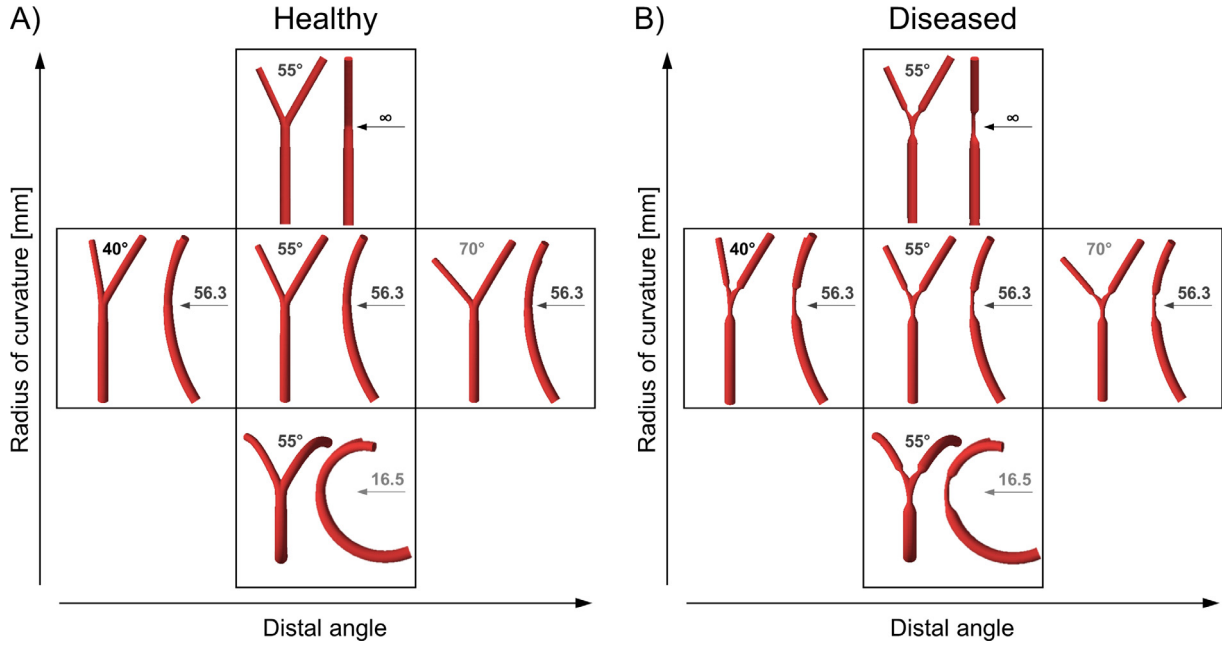

Fig. 2. Investigated coronary bifurcation models: (A) healthy and (B) diseased geometries.

have been proven to reduce the likelihood of flow disturbances at the bifurcation (Gallo et al., 2012).

While the interplay between geometry, near-wall and intravascular flow features has been widely studied in carotid bifurcations, less is known about the diseased coronary bifurcations. Indeed, several studies focused on the influence on near-wall descriptors ascribable to anatomical features, such as the presence of stenosis at varying locations and with different severity/extension (Frattolin et al., 2015; Pagiatakis et al., 2015; Peng et al., 2016; Pinto and Campos, 2016), bifurcation angle (Beier et al., 2016;

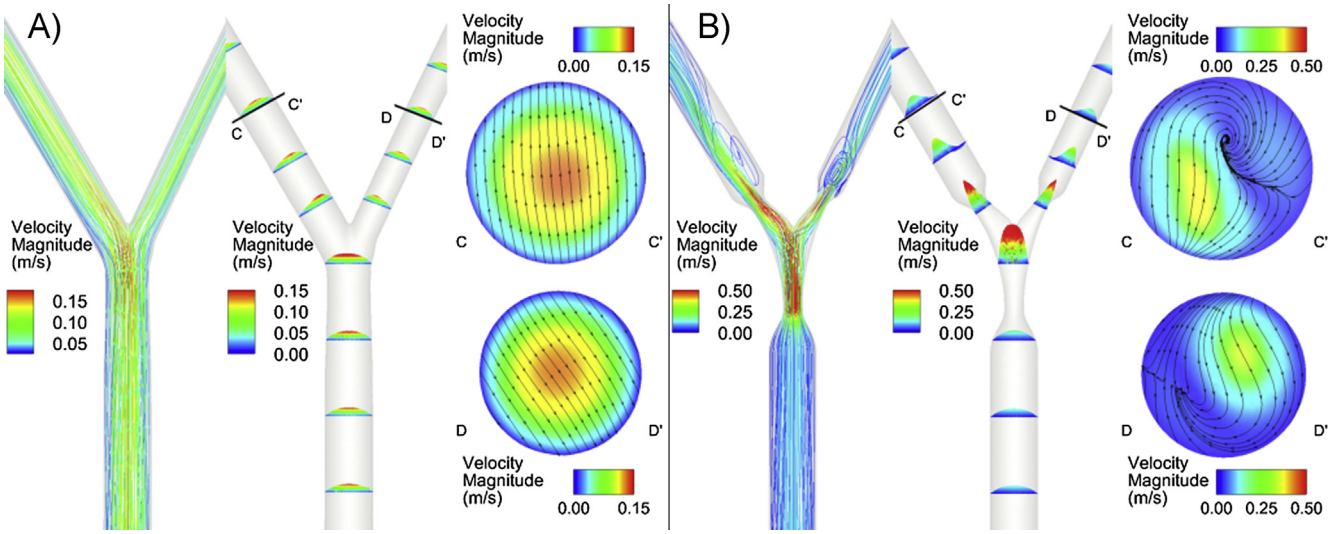

Fig. 3. Intravascular hemodynamics of a representative bifurcation model without (A) and with (B) stenosis (case with 55° bifurcation angle and curvature radius of 56.3 mm): time-averaged velocity streamlines (left), velocity profiles on selected cross-section normal to the vessel centerline (center), and velocity contours with in-plane velocity vectors at a cross-section of the distal main branch and side branch, respectively (right).

Chaichana et al., 2011; Dong et al., 2015; Liu et al., 2015), curvature (Liu et al., 2015; Peng et al., 2016), and tortuosity (Malvè et al., 2014; Peng et al., 2016). For example, Vorobtsova et al. (2016) investigated the effect of tortuosity on coronary flow features, including WSS-based descriptors and helical flow intensity, though only in the non-bifurcated segments of patient-specific coronary trees.

The aim of the present study is to investigate the influence of peculiar coronary bifurcation anatomical features on both near-wall and intravascular flow features. In particular, the impact of stenosis presence, bifurcation angle, and curvature on local hemodynamics is analyzed by performing CFD simulations on a population-based, idealized model of coronary bifurcation. Such an idealized model-based approach will enable, by varying one specific geometrical feature at a time while keeping the others constant, to clearly identify if and to which extent anatomic features promote atheroprotective or atherosusceptible hemodynamic phenotypes.

2. Material and methods

2.1. Coronary bifurcation models

A parametric model of a coronary bifurcation representing the left anterior descending (LAD) coronary artery with its diagonal branch was created using the open-source software PyFormex (http://www.nongnu.org/pyformex/) (Fig. 1), as detailed elsewhere (Chiastra et al., 2016; Iannaccone et al., 2016). Briefly, the diameter of the proximal main branch (MB) is 3.30 mm (Medrano-Gracia et al., 2016) while the diameters of the distal MB and the side branch (SB) are 2.77 mm and 2.10 mm, respectively, in agreement with the Finet's law (Finet et al., 2008). The angle between the proximal MB and the SB was set to 150° (Medrano-Gracia et al., 2016) while the distal bifurcation angle 'α' was varied within the physiological range (Godino et al., 2010; Onuma et al., 2008). In particular, models with bifurcation angles of 40°, 55°, and 70° were created. The curvature of the coronary bifurcation due to the presence of the heart was taken into account by bending the model on a sphere of radius 'R'. A physiological curvature radius was considered (R = 56.3 mm) (Pivkin et al., 2005) as well as two extreme values ($R = \infty$, i.e. absence of curvature, and R = 16.5 mm). Both healthy (i.e. without stenosis) and diseased (i.e. with stenosis) bifurcation models were analyzed. The diseased models are characterized by 60% diameter stenosis in each branch, thus representing a (1, 1, 1) lesion according to Medina classification (Medina et al., 2006), a widely accepted clinical classification for coronary bifurcations that assigns a binary value (0, 1) to each branch depending on whether they have less than (0) or more than (1) 50% lesion. Here a (1, 1, 1) Medina classification lesion was examined as it is considered the most critical geometry. The lesion is 12 mm long and eccentric, with plaque located at the inner arc of the vessel (Fig. 1B).

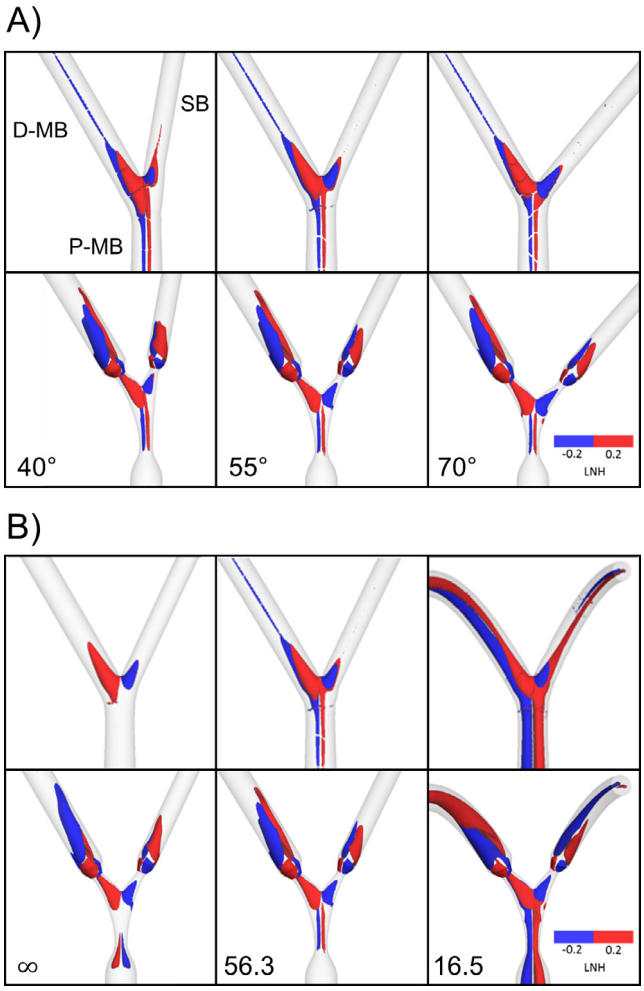

Fig. 4. Isosurfaces of local normalized helicity (LNH) for cases with (A) different distal bifurcation angle and 56.3 mm radius of curvature, and (B) different radius of curvature and bifurcation angle equal to 55°. In both panels healthy (top) and diseased (bottom) bifurcation models are shown. Positive (red color) and negative (blue color) LNH values indicate right-handed and left-handed rotating fluid structures along the main flow direction, respectively. (For interpretation of the references to colour in this figure legend, the reader is referred to the web version of this article.)

In summary, 10 coronary bifurcation models were investigated (Fig. 2) by combining 3 distal angles and 3 curvature radii, both for the healthy and the diseased coronary bifurcation models.

The bifurcation models were discretized using ICEM CFD (ANSYS Inc., Canonsburg, PA, USA). A tetrahedral grid with a prism layer and finer elements at the stenosis region was generated. The mesh cardinality was ~2,500,000 after a mesh independence study (Chiastra et al., 2016).

2.2. Computational hemodynamics

For all cases under study, the governing equations of unsteady, incompressible fluid motion were solved by using the finite volume method-based commercial software Fluent (ANSYS Inc.). A typical human LAD flow waveform (Davies et al., 2006) was imposed at the inlet as a plug velocity profile. The mean flow rate was 43.2 ml/min, in agreement with *in vivo* flow measurements in the human LAD (Kessler et al., 1998). A flow-split of 65%:35% for the distal MB and SB, respectively, was applied at the outlets. This value was calculated using the relation between the diameter ratio and the flow ratio of daughter branches under the assumption of absence of stenosis (van der Giessen et al., 2011). The flow-split was maintained constant in the diseased bifurcation models in order to focus the analysis only on the impact of geometrical features on the local hemodynamics. The arterial wall was assumed as rigid, subjected to the no-slip condition. Blood was modelled as a non-Newtonian fluid using the Carreau model with a density of 1060 kg/m^3 (Caputo et al., 2013). The flow was assumed as laminar (maximum Reynolds number = ~330 at the PMB stenosis of the diseased cases).

Details about the solver settings are reported in the Supplementary Materials.

2.3. Analysis of the results

Intravascular fluid structures were investigated in terms of helical flow topology and content. Helicity intensity h_2 and helical rotation balance h_4 were calculated in the entire model, in the proximal MB, in the distal MB, and in the SB (Fig. 1). According to (Gallo et al., 2015, 2012; Morbiducci et al., 2013), these helical-based bulk flow descriptors are defined as:

$$h_2 = \frac{1}{TV}\int_T \int_V |\vec{v}\cdot\vec{\omega}|dVdt \tag{1}$$

$$h_4 = \frac{\left|\int_T \int_V \vec{v}\cdot\vec{\omega}dVdt\right|}{\int_T \int_V |\vec{v}\cdot\vec{\omega}|dVdt} \tag{2}$$

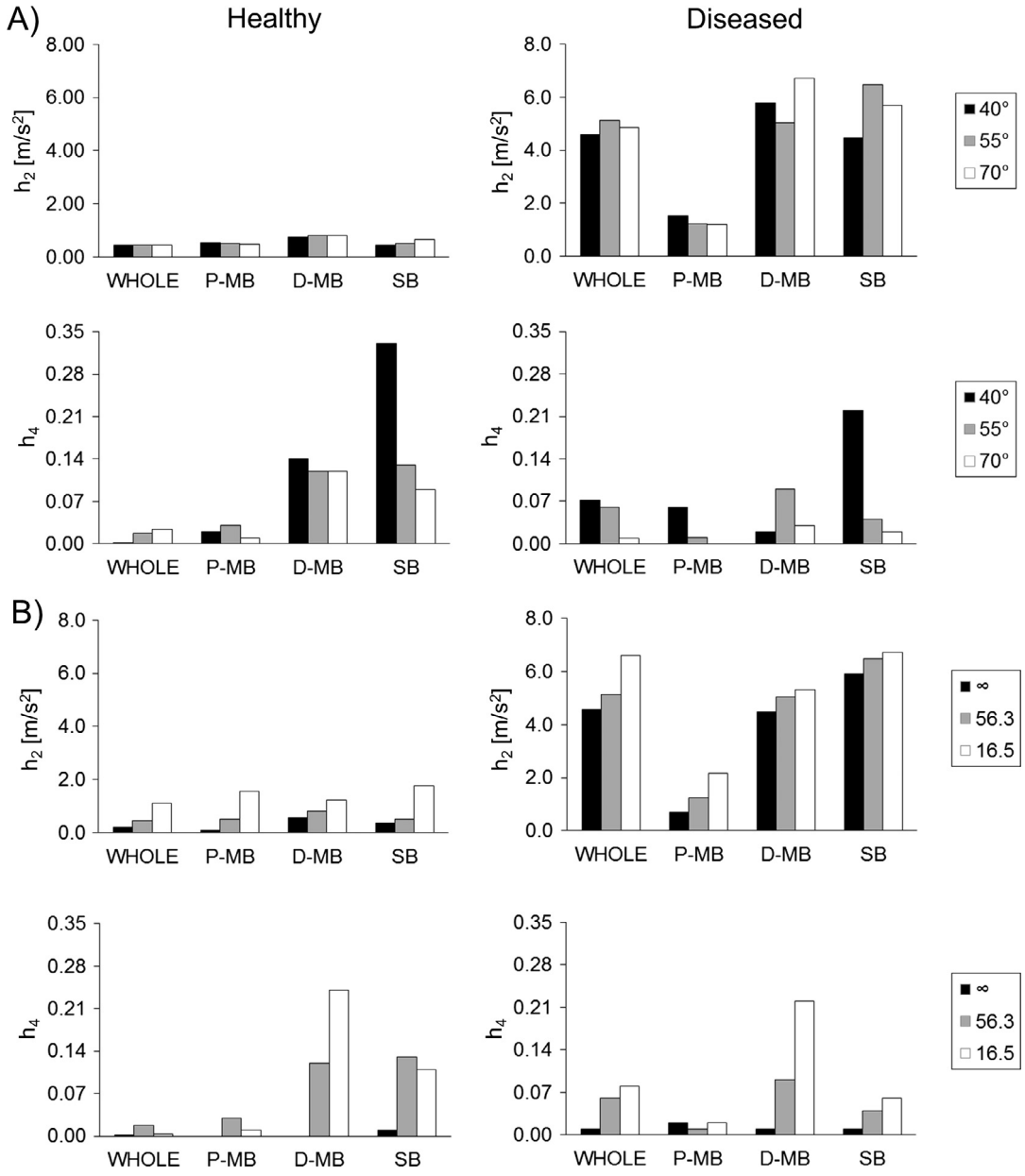

Fig. 5. Quantitative analysis of intravascular flow. Helicity intensity (h_2) and helical rotation balance (h_4) values in healthy (left panel) and diseased (right panel) models with (A) different distal bifurcation angle value and (B) different curvature radius value. The analysis was performed on the entire domain (WHOLE), proximal main branch (P-MB), distal main branch (D-MB), and side branch (SB).

where $\vec{v}$ is the velocity vector, $\vec{\omega}$ is the vorticity vector, V is the volumetric fluid domain of interest, and T is the cardiac cycle. Helicity intensity is an indicator of the total amount of helical flow while the helical rotation balance measures the strength of relative rotations of helical flow structures. Furthermore, the local normalized helicity (LNH) was calculated to visualize the spiral flow patterns that develop inside the bifurcation models (Morbiducci et al., 2007). LNH is defined as:

$$\mathrm{LNH} = \frac{\vec{v} \cdot \vec{\omega}}{|\vec{v}| \cdot |\vec{\omega}|} = \cos\gamma \tag{3}$$

where γ is the angle between the velocity and the vorticity vectors. Positive (negative) values of LNH indicate right-handed (left-handed) rotating structures.

Near-wall hemodynamics was evaluated in terms of time-averaged WSS (TAWSS), oscillatory shear index (OSI), and relative residence time (RRT), a hemodynamic descriptor able to identify regions of low and oscillatory WSS (Himburg et al., 2004). In particular, the fraction of the luminal area exposed to TAWSS < 0.4 Pa, OSI > 0.2, and RRT > 4.17 Pa^{-1} (as a consequence of threshold values set for TAWSS and OSI) was calculated in the entire model, in the proximal MB, in the distal MB, and in the SB (Fig. 1). Low TAWSS and high OSI values are known to stimulate a proatherogenic endothelial phenotype (He and Ku, 1996; Malek et al., 1999). Definitions of near-wall descriptors are reported in the Supplementary Materials.

3. Results

3.1. Intravascular flow

The stenosis presence in the bifurcation region strongly affects the intravascular hemodynamics, where jet-like structures are visible in the distal MB and SB, respectively (Fig. 3). Recirculation regions are also evident in the daughter branches downstream of the stenosis.

The complexity of the hemodynamics establishing within the coronary bifurcation can be appreciated by visualizing LNH isosurfaces (Fig. 4). Well-distinguished counter-rotating helical flow structures are the emerging hemodynamic feature at the bifurcation in all investigated models. In the healthy cases, mild differences can be appreciated in helical flow structures in the SB because of different bifurcation angles (Fig. 4A-top). The presence of the lesion alters the intravascular flow topology (Fig. 4A-bottom), resulting in helical flow structures that originate in the bifurcation region and develop into the daughter branches, elongating more downstream into the distal MB than the SB. The differences between the cases with increasing bifurcation angle are attenuated compared to the healthy geometries (Fig. 4A-bottom).

The effect of curvature radius on helical flow structures is shown in Fig. 4B. The analysis of the healthy cases highlights that increasing curvature plays a role in promoting helical fluid structures transported to the bifurcation. In particular, the helical flow establishing by the curved proximal MB enters the bifurcation with an inertial contribution that amplifies the helicity intensity in that region (Gallo et al., 2015). A further source to helical flow generation is given by the local curvature all along the bifurcation region and downstream of it, leading to the onset of Dean-like effects (Morbiducci et al., 2011) affecting the intravascular fluid structures.

The quantitative analysis of the helicity confirms the qualitative observations (Fig. 5). In general, the bifurcation angle moderately affects helical flow features. In healthy cases, helicity intensity shows a negligible increase in the whole domain and in the daughter branches with the bifurcation angle (Fig. 5A-top). Diseased cases exhibit helicity intensity h_2 one order of magnitude higher than healthy cases, with a not monotonic trend for increasing bifurcation angles (Fig. 5A-top). Globally, helical flow structures are symmetrical, as demonstrated by the nearly 0 values of the helical rotation balance in the entire model (Fig. 5A-bottom). However, the values of h_4 in the distal MB and SB indicate that helical flow structures are asymmetric in those segments, in particular in the SB of the 40° bifurcation angle model (Fig. 5A-bottom). The helical rotation balance values (Fig. 5A-bottom) suggest that the presence of the lesion makes helical flow structures more symmetrical in the distal MB and SB, when compared to the corresponding healthy cases. The most asymmetric helical flow structures are present in the SB of the 40° bifurcation angle also in the diseased cases.

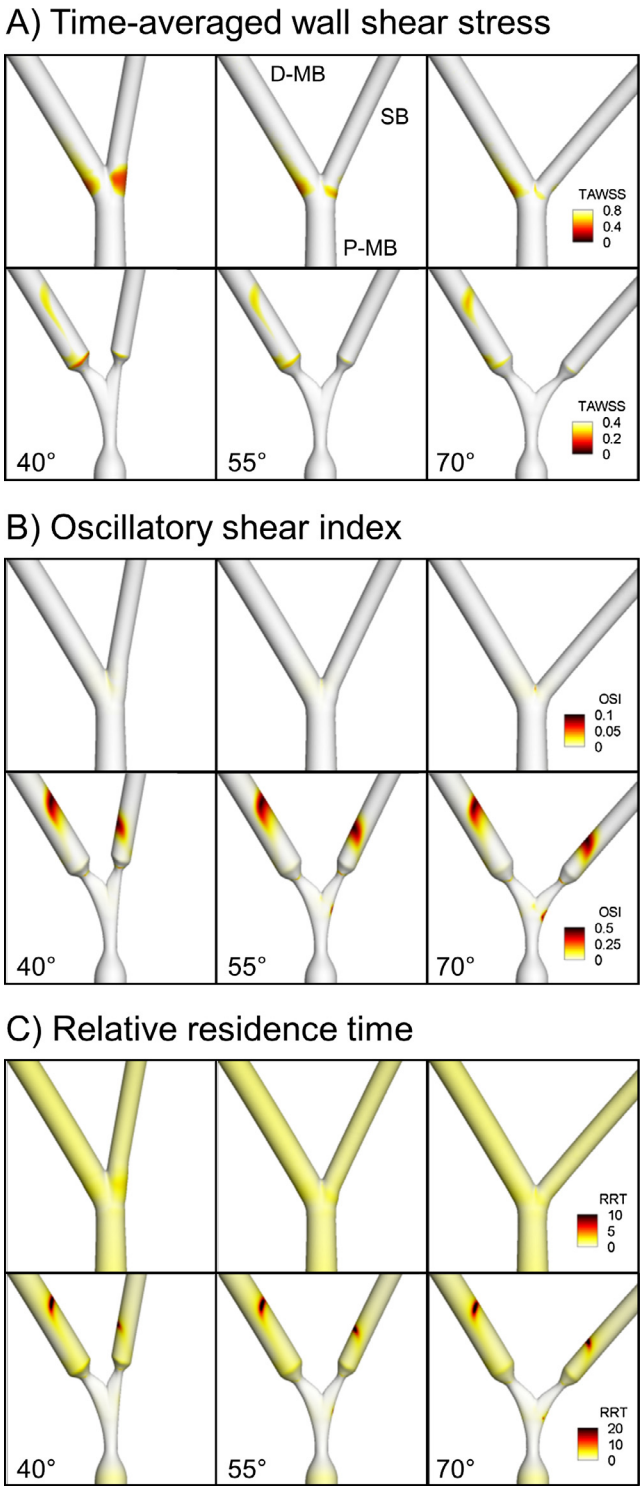

Fig. 6. Contour maps of near-wall quantities for cases with different distal bifurcation angle: A) time-averaged wall shear stress (TAWSS); B) oscillatory shear index (OSI); C) relative residence time (RRT). For each quantity, both healthy (top row) and diseased (bottom row) bifurcation models are shown. The position of the proximal main branch (P-MB), distal main branch (D-MB), and the side branch (SB) is indicated in (A).

Table 1
Relative luminal surface area exposed to time-averaged wall shear stress (TAWSS) lower than 0.4 Pa, oscillatory shear index (OSI) higher than 0.2, and relative residence time (RRT) higher than 4.17 Pa^{-1} for healthy cases with different bifurcation angle and radius of curvature.

	Relative surface area [%]											
	TAWSS < 0.4 Pa				OSI > 0.2				RRT > 4.17 Pa^{-1}			
	WHOLE	P-MB	D-MB	SB	WHOLE	P-MB	D-MB	SB	WHOLE	P-MB	D-MB	SB
Bifurcation angle [°]												
40°	0.42	0.00	0.47	1.50	0.00	0.00	0.00	0.00	0.00	0.00	0.00	0.00
55°	0.07	0.00	0.24	0.00	0.00	0.00	0.00	0.00	0.00	0.00	0.00	0.00
70°	0.00	0.00	0.00	0.00	0.00	0.00	0.00	0.00	0.00	0.00	0.00	0.00
Curvature radius [mm]												
∞	0.00	0.00	0.00	0.00	0.00	0.00	0.00	0.00	0.00	0.00	0.00	0.00
56.3	0.07	0.00	0.24	0.00	0.00	0.00	0.00	0.00	0.00	0.00	0.00	0.00
16.5	0.07	0.00	0.00	0.00	0.00	0.00	0.00	0.00	0.00	0.00	0.00	0.00

WHOLE – entire lumen; P-MB – proximal main branch; D-MB – distal main branch; SB – side branch.

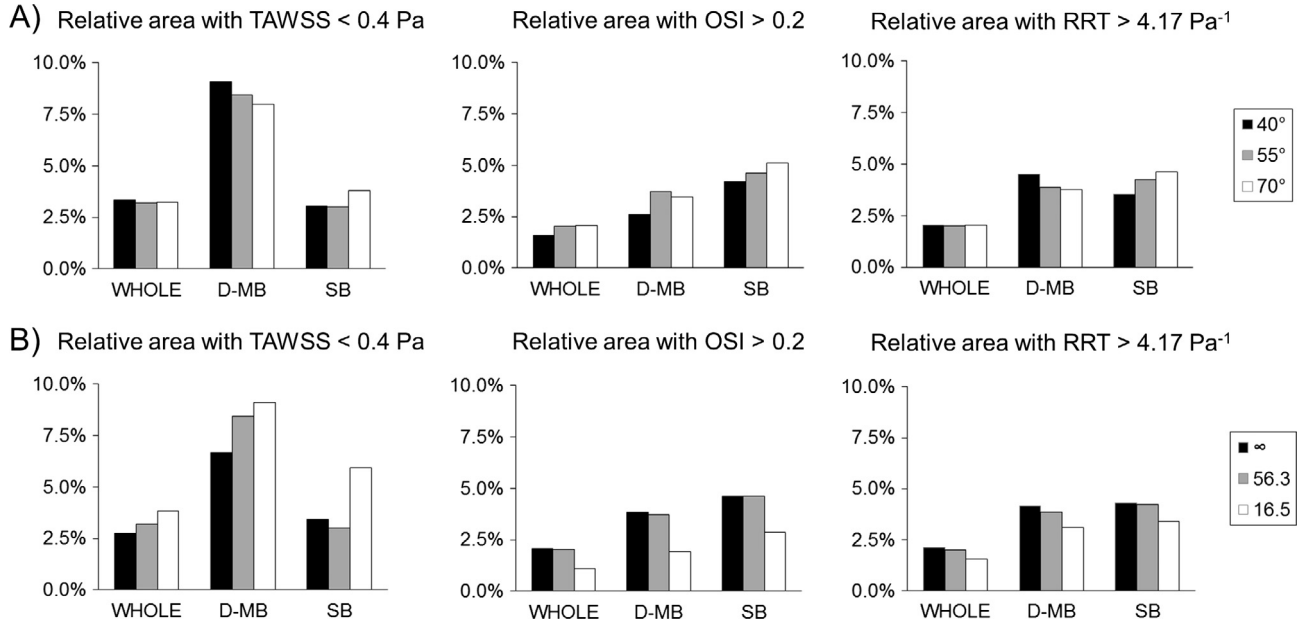

Fig. 7. Bar diagrams of relative luminal area exposed to time-averaged wall shear stress (TAWSS) lower than 0.4 Pa, oscillatory shear index (OSI) higher than 0.2, and relative residence time (RRT) higher than 4.17 Pa^{-1} for diseased cases with different (A) distal bifurcation angle and (B) radius of curvature. The analysis was performed on the entire lumen (WHOLE), distal main branch (D-MB), and side branch (SB).

Data in Fig. 5B-top confirm the role of the decreasing curvature radius in amplifying helicity intensity h_2 in all bifurcation branches with a monotonic trend for both healthy and diseased cases. The decreasing curvature radius markedly modifies also flow topology, breaking the symmetry of the helical structures in the distal MB (Fig. 5B-bottom), which is less so the case for the SB.

3.2. Near-wall hemodynamics

In the healthy models with different bifurcation angle, low TAWSS is located at the ostium of the daughter branches, opposite to the carina (Fig. 6A), due to the presence of flow separation regions (Fig. 3A). Although the observed differences are very small, the fraction of the entire lumen surface area exposed to low TAWSS slightly decreases with increasing bifurcation angle (Table 1). As expected, the presence of the lesion leads to different patterns of low TAWSS distribution at the luminal surface (Fig. 6A). In particular, in the diseased cases with different bifurcation angle, the surface area exposed to low TAWSS is mainly located at the distal MB (Fig. 6A). However, the surface area exposed to low TAWSS increased only to ~3.3% in diseased cases, as compared to healthy ones (Fig. 7A).

Considering OSI and RRT, in all healthy cases with different bifurcation angle the surface area exposed to high OSI is negligible (Fig. 6B, Table 1) and RRT is always lower than 3 Pa^{-1} (Fig. 6C, Table 1). Conversely, surface areas exposed to atherosusceptible OSI and RRT values can be observed in diseased cases at the distal MB and at the SB (Fig. 6B and C), close to the reattachment point of the recirculation regions. Quantitatively, surface areas exposed to high OSI and RRT values are similar among the investigated diseased cases, showing a poor dependence on the bifurcation angle (Fig. 7A).

The curvature radius has negligible impact on the distributions of WSS-based descriptors at the lumen of the healthy bifurcations (Fig. 8). Qualitatively, areas exposed to low TAWSS slightly increase with lowering curvature radius. However, the relative area with TAWSS lower than 0.4 Pa is ~0% in the three investigated healthy cases (Table 1). Additionally, the surface area exposed to atherosusceptible OSI values is almost null while RRT is lower than 3 Pa^{-1} everywhere (Fig. 8B and C, Table 1). Distributions of WSS-based descriptors of the diseased cases are moderately affected

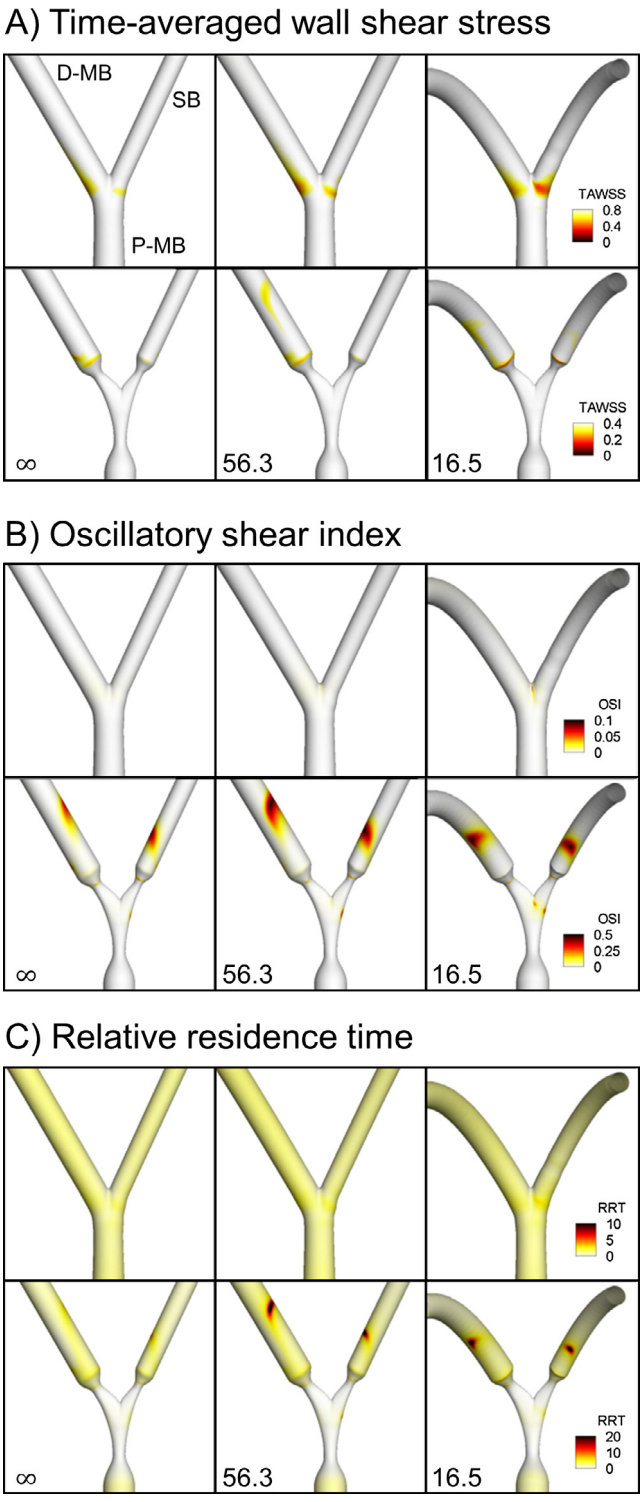

Fig. 8. Contour maps of near-wall quantities for cases with different radius of curvature: A) time-averaged wall shear stress (TAWSS); B) oscillatory shear index (OSI); C) relative residence time (RRT). For each quantity, both healthy (top row) and diseased (bottom row) bifurcation models are shown. The position of the proximal main branch (P-MB), distal main branch (D-MB), and side branch (SB) is indicated in (A).

by the curvature radius (Fig. 8). In detail, a smaller curvature radius (i) increases the surface area exposed to low TAWSS, in particular in the distal MB (Fig. 7B); (ii) decreases the surface area exposed to high OSI and RRT values (Fig. 7B).

4. Discussion

Geometry has long been recognized as possible risk factor for plaque localization, by virtue of its influence on intra-vascular and near-wall flow patterns (Ding et al., 1997; Morbiducci et al., 2016). The present study contributes to identify if and to which extent anatomic features promote atheroprotective or atherosusceptible hemodynamic phenotypes at the LAD/diagonal bifurcation. The endeavor to link geometry and atherosusceptibility is based on a strong clinical motivation, as geometric features can be easily and reliably measured using standard clinical imaging facilities. On the other hand, the studied hemodynamic phenotypes are hard to access in clinical practice (Morbiducci et al., 2016). Therefore, the identification of practical measurable geometric features able to predict hemodynamic phenotypes represents a first step toward the identification of geometry-based local risk factors for risk stratification in the population, identifying subjects with greater susceptibility for atherosclerosis in the considered region. For coronary arteries, several investigations focused at the left main bifurcation, i.e. where the LAD and the left circumflex artery (LCx) stem from the left main coronary artery (Morbiducci et al., 2016). For instance, at this bifurcation the presence of plaques in the LAD segment correlated with both the planarity of the bifurcation and the bifurcation angle between LAD and LCx (Ding et al., 1997). Conversely, the LAD/diagonal bifurcation has been less explored. In this study, inspired by the approach recently applied to the carotid bifurcation (Gallo et al., 2012), we considered healthy and diseased population-based, idealized models of coronary LAD/diagonal bifurcation with varying bifurcation angle and curvature. In detail, helicity-based description was adopted to characterize intravascular flow features. Such a description has the purpose of extending and complementing the WSS-based analysis of hemodynamics and its well-known relationship with plaque initiation (Wentzel et al., 2012). It is motivated by recent findings demonstrating (i) an atheroprotective role of specific helical flow structures, although in the carotid bifurcation (Gallo et al., 2015, 2012), and (ii) that helical flow significantly reduces the flow instability caused by a stenosis (Linge et al., 2014; Stonebridge et al., 2004). Although the role of helical flow in plaque genesis and progression at LAD/diagonal bifurcation is still not fully elucidated (Morbiducci et al., 2016), recent observations in the LAD coronary artery showed a helical layout of roughness ridges (Burton et al., 2016), which can be linked to the establishment of coronary helical flow patterns (Van Langenhove et al., 2000). Additionally, the here presented WSS-based analysis considers low and oscillatory WSS in light of atherosclerosis initiation and early progression.

A sketch summarizing the present findings is shown in Fig. 9. While the effect of different bifurcation angles and curvature radii on the considered hemodynamic parameters is negligible for healthy cases, greater variations are shown by diseased cases. Both vessel curvature and stenosis presence influence the generation and transport of helical flow structures. Mechanistically, an increasing vessel curvature promotes secondary flows, ultimately influencing the composition of blood translational and rotational motions (Gallo et al., 2015). In healthy cases, helical flow topology results mainly from the curvature of the vessel (Fig. 4B-top). In diseased cases, the impact of curvature on helical flow structures piles up with the helicity generated as a consequence of the lumen reduction (Grigioni et al., 2005). This latter plays the main role in helical flow generation, as it is responsible of the highest variations in helicity intensity: in the diseased cases, h_2 is one of order of magnitude higher than in the corresponding healthy geometries (Fig. 5D). Furthermore, while helical flow structures are symmetrical in the planar bifurcation ($h_4 \sim 0$), they are asymmetric in the curved cases (i.e. higher helical rotation balance h_4) (Fig. 5D). It is

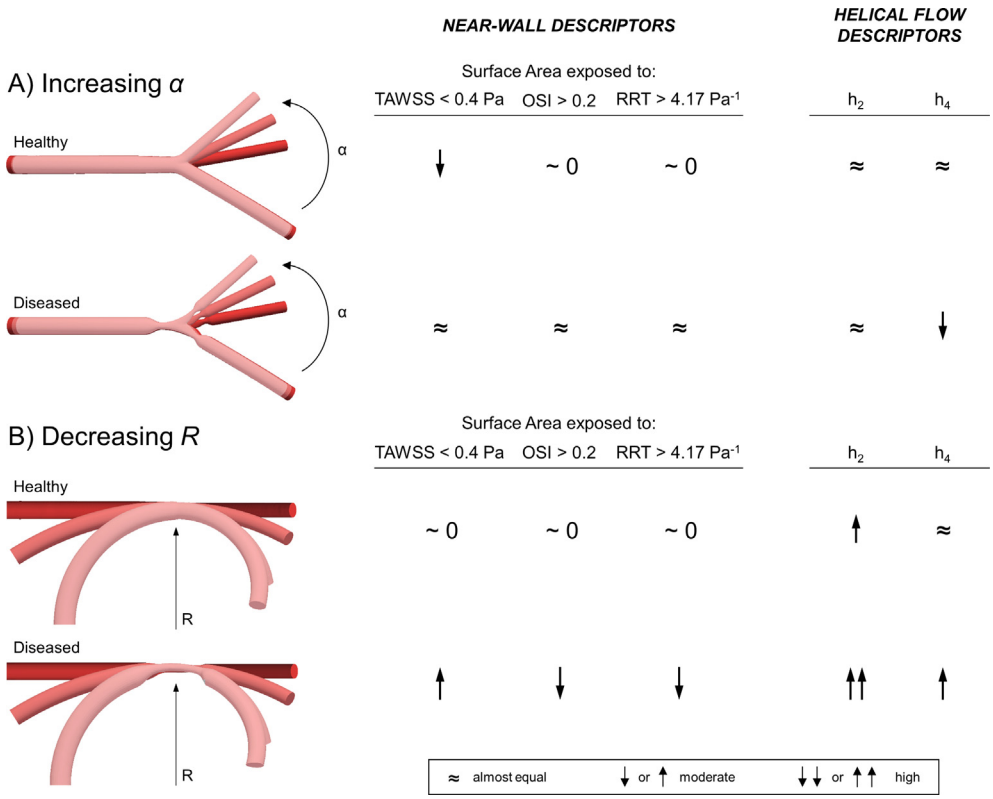

Fig. 9. Qualitative scheme summarizing changes in terms of near-wall and helical flow descriptors because of (A) increasing bifurcation angle and (B) decreasing radius of curvature for healthy and diseased bifurcation models. The findings refer to the analyses on the whole fluid domain.

worth noting that 10 out the 18 possible coronary bifurcation models were examined (Fig. 2). The remaining geometrical combinations were not examined because bifurcation angle is shown to have a minor effect on local hemodynamics (Figs. 4 and 5).

Previous analyses of intravascular flow in coronary bifurcations are limited. While some studies focused on non-bifurcated segments of coronary arteries (Van Langenhove et al., 2000; Vorobtsova et al., 2016), Chiastra et al. (2016) investigated stenosed LAD coronary bifurcation models with different bifurcation angles, though under steady-state, hyperemia condition. Unlike our findings, the researchers observed that helicity intensity moderately increases as the bifurcation angle becomes wider in Medina (1, 1, 1) bifurcations with 60% stenosis. However, this monotonically increasing trend was found under steady hyperemic flow conditions, which are characterized by a mean flow-rate at least three-times higher than at rest. That is to say, a higher Reynolds number exacerbates the influence of geometry on helical flow, through the reduction of the relative influence of viscous forces with respect to centrifugal and inertial forces.

Regarding the near-wall hemodynamics, our results shows that low TAWSS, high OSI, and high RRT are located at the lateral walls opposite to the carina in healthy bifurcations and at the daughter branches downstream of the stenosis in diseased cases, in agreement with previous studies (Chaichana et al., 2011; Huo et al., 2012; Liu et al., 2015; Malvè et al., 2014; Peng et al., 2016; Pinto and Campos, 2016). Quantitative comparison of surface area exposed to adverse near-wall descriptors cannot be performed as previous works investigated the left main coronary bifurcation, which is characterized by larger diameter and higher flow rates than the LAD. In this study, limited exposure to oscillatory shear is observed in healthy bifurcations because of hemodynamics characterized by low Reynolds and Womersley numbers (Re_{max} = 136, Wo = 2.4, respectively). Conversely, larger lumen areas with adverse WSS-based descriptors are found in the diseased cases.

In general, our results show that the bifurcation angle has a minor impact on surface areas exposed to adverse near-wall descriptors (Fig. 9), confirming previous investigations (Beier et al., 2016; Dong et al., 2015). Regions with low TAWSS are found to moderately reduce only in healthy bifurcations with higher angle, as previously reported (Beier et al., 2016; Chaichana et al., 2011; Liu et al., 2015; Malvè et al., 2014). In agreement with our finding of a moderate increase in area exposed to low and oscillatory WSS at the SB of diseased models with different bifurcation angles, it has been observed that wider angle may induce plaque proliferation and lead to more severe stenosis at the SB ostium, with a consequent higher risk of SB occlusion (Zhang and Dou, 2015).

Additionally, this study highlights that the cardiac curvature radius moderately affects the distributions of WSS-based descriptors of the diseased cases (Fig. 9). In accordance with previous findings (Liu et al., 2015), a lower curvature radius is associated with larger areas exposed to low TAWSS, in particular at the inner side of the curvature, and smaller areas exposed to high OSI and RRT. It is worth noting that in carotid bifurcation an increase of helicity intensity corresponded to a decrease in the exposure to both low and oscillatory WSS (Gallo et al., 2012). While the relationship between helicity intensity and oscillatory WSS is echoed here, this is not the case for the exposure to low TAWSS. This may be ascribed to the fact that in bifurcation models considered here helical flow is generated by the out-of-plane curvature with respect to the bifurcation plane, while in carotid bifurcation helical flow is promoted primarily by planar curvature (Bijari et al., 2014, 2012).

This study suffers from some limitations. In stenosed coronary bifurcations, blood flow division between daughter branches is

governed by local resistances, which depend on stenosis severity, and downstream resistances, which are related to the patient-specific myocardium condition. This may lead to a possible different flow-split than the healthy bifurcations. However, in our analyses the same flow split was applied as outlet boundary condition in both healthy and diseased models, in order to investigate exclusively the impact of coronary bifurcation geometric features on intravascular and near-wall hemodynamics. In principle, inflow boundary condition is affected by the local resistance at the stenosis: however, previous studies demonstrated that a variation in the inflow occurs for stenosis severity greater that 70% (Pietrabissa et al., 1996). Moreover, the vessel wall was assumed as rigid. This assumption may lead to an overestimation of the TAWSS (Dong et al., 2015; Malvè et al., 2012), even though the TAWSS spatial distribution remains substantially similar between rigid-wall and fluid-structure interaction approaches (Malvè et al., 2012). Finally, the cardiac-induced motion of the coronary bifurcation was neglected, as previous investigations reported it as only moderately influencing near-wall coronary hemodynamics (Hasan et al., 2013; Prosi et al., 2004; Theodorakakos et al., 2008; Zeng et al., 2003).

5. Conclusions

In this study, CFD simulations were performed on a population-based, idealized model of stenosed and unstenosed coronary bifurcations to evaluate the impact of peculiar anatomic features (bifurcation angle and curvature) on local hemodynamics. Results show that bifurcation angle has a minor effect on the calculated hemodynamic variables in both healthy and diseased cases. Instead, curvature radius influences the generation and transport of helical flow structures. Smaller curvature radius is associated with higher helicity intensity in both healthy and diseased cases, with the diseased bifurcation models exhibiting helicity intensity values one order of magnitude higher than the corresponding healthy cases due to the stenosis presence. Furthermore, curvature radius moderately affects the near-wall hemodynamics of the diseased cases. In detail, smaller curvature radius leads to larger lumen area exposed to low TAWSS and smaller lumen area exposed to high OSI and RRT.

In conclusion, the proposed controlled benchmark allows investigating the effect of various geometrical features on local hemodynamics, highlighting that cardiac curvature influences near wall and intravascular hemodynamics, while bifurcation angle has a minor effect.

Conflict of interest

The authors have no professional or financial conflicts of interest to disclose.

Acknowledgements

C. Chiastra and J.J. Wentzel are supported by the ERC starting grant (No. 310457, BioCCora).

Appendix A. Supplementary material

Supplementary data associated with this article can be found, in the online version, at http://dx.doi.org/10.1016/j.jbiomech.2017.04.016.

References

Antoniadis, A.P., Giannopoulos, A.A., Wentzel, J.J., Joner, M., Giannoglou, G.D., Virmani, R., Chatzizisis, Y.S., 2015. Impact of local flow haemodynamics on atherosclerosis in coronary artery bifurcations. EuroIntervention 11 (Suppl V), V18–22. http://dx.doi.org/10.4244/EIJV11SVA4.

Beier, S., Ormiston, J., Webster, M., Cater, J., Norris, S., Medrano-Gracia, P., Young, A., Cowan, B., 2016. Impact of bifurcation angle and other anatomical characteristics on blood flow – a computational study of non-stented and stented coronary arteries. J. Biomech. 49, 1570–1582. http://dx.doi.org/10.1016/j.jbiomech.2016.03.038.

Bijari, P.B., Antiga, L., Gallo, D., Wasserman, B.A., Steinman, D.A., 2012. Improved prediction of disturbed flow via hemodynamically-inspired geometric variables. J. Biomech. 45, 1632–1637. http://dx.doi.org/10.1016/j.jbiomech.2012.03.030.

Bijari, P.B., Wasserman, B.A., Steinman, D.A., 2014. Carotid bifurcation geometry is an independent predictor of early wall thickening at the carotid bulb. Stroke 45, 473–478. http://dx.doi.org/10.1161/STROKEAHA.113.003454.

Burton, H.E., Freij, J.M., Espino, D.M., 2016. Dynamic viscoelasticity and surface properties of porcine left anterior descending coronary arteries. Cardiovasc. Eng. Technol. http://dx.doi.org/10.1007/s13239-016-0288-4.

Caputo, M., Chiastra, C., Cianciolo, C., Cutrì, E., Dubini, G., Gunn, J., Keller, B., Migliavacca, F., Zunino, P., 2013. Simulation of oxygen transfer in stented arteries and correlation with in-stent restenosis. Int. J. Numer. Method. Biomed. Eng. 29, 1373–1387. http://dx.doi.org/10.1002/cnm.2588.

Chaichana, T., Sun, Z., Jewkes, J., 2011. Computation of hemodynamics in the left coronary artery with variable angulations. J. Biomech. 44, 1869–1878. http://dx.doi.org/10.1016/j.jbiomech.2011.04.033.

Chiastra, C., Iannaccone, F., Grundeken, M.J., Gijsen, F.J.H., Segers, P., De Beule, M., Serruys, P.W., Wykrzykowska, J.J., van der Steen, A.F.W., Wentzel, J.J., 2016. Coronary fractional flow reserve measurements of a stenosed side branch: a computational study investigating the influence of the bifurcation angle. Biomed. Eng. Online 15, 91. http://dx.doi.org/10.1186/s12938-016-0211-0.

Davies, J.E., Whinnett, Z.I., Francis, D.P., Manisty, C.H., Aguado-Sierra, J., Willson, K., Foale, R.a., Malik, I.S., Hughes, A.D., Parker, K.H., Mayet, J., 2006. Evidence of a dominant backward-propagating "suction" wave responsible for diastolic coronary filling in humans, attenuated in left ventricular hypertrophy. Circulation 113, 1768–1778. http://dx.doi.org/10.1161/CIRCULATIONAHA.105.603050.

Ding, Z., Biggs, T., Seed, W.A., Friedman, M.H., 1997. Influence of the geometry of the left main coronary artery bifurcation on the distribution of sudanophilia in the daughter vessels. Arterioscler. Thromb. Vasc. Biol. 17, 1356–1360.

Dong, J., Sun, Z., Inthavong, K., Tu, J., 2015. Fluid-structure interaction analysis of the left coronary artery with variable angulation. Comput. Methods Biomech. Biomed. Eng. 18, 1500–1508. http://dx.doi.org/10.1080/10255842.2014.921682.

Finet, G., Gilard, M., Perrenot, B., Rioufol, G., Motreff, P., Gavit, L., Prost, R., 2008. Fractal geometry of arterial coronary bifurcations: a quantitative coronary angiography and intravascular ultrasound analysis. EuroIntervention 3, 490–498.

Frattolin, J., Zarandi, M.M., Pagiatakis, C., Bertrand, O.F., Mongrain, R., 2015. Numerical study of stenotic side branch hemodynamics in true bifurcation lesions. Comput. Biol. Med. 57, 130–138. http://dx.doi.org/10.1016/j.compbiomed.2014.11.014.

Gallo, D., Steinman, D.A., Bijari, P.B., Morbiducci, U., 2012. Helical flow in carotid bifurcation as surrogate marker of exposure to disturbed shear. J. Biomech. 45, 2398–2404. http://dx.doi.org/10.1016/j.jbiomech.2012.07.007.

Gallo, D., Steinman, D.A., Morbiducci, U., 2015. An insight into the mechanistic role of the common carotid artery on the hemodynamics at the carotid bifurcation. Ann. Biomed. Eng. 43, 68–81. http://dx.doi.org/10.1007/s10439-014-1119-0.

Godino, C., Al-Lamee, R., La Rosa, C., Morici, N., Latib, A., Ielasi, A., Di Mario, C., Sangiorgi, G.M., Colombo, A., 2010. Coronary left main and non-left main bifurcation angles: how are the angles modified by different bifurcation stenting techniques? J. Interv. Cardiol. 23, 382–393. http://dx.doi.org/10.1111/j.1540-8183.2010.00562.x.

Grigioni, M., Daniele, C., Morbiducci, U., Del Gaudio, C., D'Avenio, G., Balducci, A., Barbaro, V., 2005. A mathematical description of blood spiral flow in vessels: application to a numerical study of flow in arterial bending. J. Biomech. 38, 1375–1386. http://dx.doi.org/10.1016/j.jbiomech.2004.06.028.

Hasan, M., Rubenstein, D.a., Yin, W., 2013. Effects of cyclic motion on coronary blood flow. J. Biomech. Eng. 135, 121002. http://dx.doi.org/10.1115/1.4025335.

He, X., Ku, D.N., 1996. Pulsatile flow in the human left coronary artery bifurcation: average conditions. J. Biomech. Eng., 118

Himburg, H.a., Grzybowski, D.M., Hazel, A.L., LaMack, J.a., LiM, X., Friedman, M.H., 2004. Spatial comparison between wall shear stress measures and porcine arterial endothelial permeability. Am. J. Physiol. Heart Circ. Physiol. 286, H1916–H1922. http://dx.doi.org/10.1152/ajpheart.00897.2003.

Huo, Y., Finet, G., Lefevre, T., Louvard, Y., Moussa, I., Kassab, G.S., 2012. Which diameter and angle rule provides optimal flow patterns in a coronary bifurcation? J. Biomech. 45, 1273–1279. http://dx.doi.org/10.1016/j.jbiomech.2012.01.033.

Iannaccone, F., Chiastra, C., Karanasos, A., Migliavacca, F., Gijsen, F.J.H., Segers, P., Mortier, P., Verhegghe, B., Dubini, G., De Beule, M., Regar, E., Wentzel, J.J., 2016. Impact of plaque type and side branch geometry on side branch compromise after provisional stent implantation. A simulation study. EuroIntervention. http://dx.doi.org/10.4244/EIJ-D-16-00498. Jaa-026 2016.

Kessler, W., Moshage, W., Galland, A., Zink, D., Achenbach, S., Nitz, W., Laub, G., Bachmann, K., 1998. Assessment of coronary blood flow in humans using phase difference MR imaging. Comparison with intracoronary Doppler flow measurement. Int. J. Card. Imaging 14, 179–186-189.

Kwak, B.R., Bäck, M., Bochaton-Piallat, M.-L., Caligiuri, G., Daemen, M.J.A.P., Davies, P.F., Hoefer, I.E., Holvoet, P., Jo, H., Krams, R., Lehoux, S., Monaco, C., Steffens, S., Virmani, R., Weber, C., Wentzel, J.J., Evans, P.C., 2014. Biomechanical factors in

atherosclerosis: mechanisms and clinical implications. Eur. Heart J. 35, 3013–3020. http://dx.doi.org/10.1093/eurheartj/ehu353.
Lassen, J.F., Holm, N.R., Banning, A., Burzotta, F., Lefèvre, T., Chieffo, A., Hildick-Smith, D., Louvard, Y., Stankovic, G., 2016. Percutaneous coronary intervention for coronary bifurcation disease: 11th consensus document from the European Bifurcation Club. EuroIntervention 12, 38–46. http://dx.doi.org/10.4244/EIJV12I1A7.
Lee, S.W., Antiga, L., Spence, J.D., Steinman, D.A., 2008. Geometry of the carotid bifurcation predicts its exposure to disturbed flow. Stroke 39, 2341–2347. http://dx.doi.org/10.1161/STROKEAHA.107.510644.
Linge, F., Hye, M.A., Paul, M.C., 2014. Pulsatile spiral blood flow through arterial stenosis. Comput. Methods Biomech. Biomed. Eng. 17, 1727–1737. http://dx.doi.org/10.1080/10255842.2013.765411.
Liu, G., Wu, J., Ghista, D.N., Huang, W., Wong, K.K.L., 2015. Hemodynamic characterization of transient blood flow in right coronary arteries with varying curvature and side-branch bifurcation angles. Comput. Biol. Med. 64, 117–126. http://dx.doi.org/10.1016/j.compbiomed.2015.06.009.
Malek, A.M., Alper, S.L., Izumo, S., 1999. Hemodynamic shear stress and its role in atherosclerosis. JAMA 282, 2035–2042. http://dx.doi.org/10.1001/jama.282.21.2035.
Malvè, M., García, a., Ohayon, J., Martínez, M.a., 2012. Unsteady blood flow and mass transfer of a human left coronary artery bifurcation: FSI vs CFD. Int. Commun. Heat Mass Transf. 39, 745–751. http://dx.doi.org/10.1016/j.icheatmasstransfer.2012.04.009.
Malvè, M., Gharib, A.M., Yazdani, S.K., Finet, G., Martínez, M.A., Pettigrew, R., Ohayon, J., 2014. Tortuosity of coronary bifurcation as a potential local risk factor for atherosclerosis: CFD steady state study based on in vivo dynamic CT measurements. Ann. Biomed. Eng. 43, 82–93. http://dx.doi.org/10.1007/s10439-014-1056-y.
Medina, A., Suárez de Lezo, J., Pan, M., 2006. A new classification of coronary bifurcation lesions. Rev. Esp. Cardiol. 59, 183. http://dx.doi.org/10.1016/S1885-5857(06)60130-8.
Medrano-Gracia, P., Ormiston, J., Webster, M., Beier, S., Young, A., Ellis, C., Wang, C., Smedby, Ö., Cowan, B., 2016. A computational atlas of normal coronary artery anatomy. EuroIntervention 12, 845–854. http://dx.doi.org/10.4244/EIJV12I7A139.
Morbiducci, U., Kok, A.M., Kwak, B.R., Stone, P.H., Steinman, D.A., Wentzel, J.J., 2016. Atherosclerosis at arterial bifurcations: evidence for the role of haemodynamics and geometry. Thromb. Haemost. 115, 484–492. http://dx.doi.org/10.1160/TH15-07-0597.
Morbiducci, U., Ponzini, R., Gallo, D., Bignardi, C., Rizzo, G., 2013. Inflow boundary conditions for image-based computational hemodynamics: impact of idealized versus measured velocity profiles in the human aorta. J. Biomech. 46, 102–109. http://dx.doi.org/10.1016/j.jbiomech.2012.10.012.
Morbiducci, U., Ponzini, R., Grigioni, M., Redaelli, A., 2007. Helical flow as fluid dynamic signature for atherogenesis risk in aortocoronary bypass. A numeric study. J. Biomech. 40, 519–534. http://dx.doi.org/10.1016/j.jbiomech.2006.02.017.
Morbiducci, U., Ponzini, R., Rizzo, G., Cadioli, M., Esposito, A., Montevecchi, F.M., Redaelli, A., 2011. Mechanistic insight into the physiological relevance of helical blood flow in the human aorta: an in vivo study. Biomech. Model. Mechanobiol. 10, 339–355. http://dx.doi.org/10.1007/s10237-010-0238-2.
Onuma, Y., Müller, R., Ramcharitar, S., van Geuns, R.-J.M., Louvard, Y., Morel, M.-A., Morice, M.-C., Davis, R., Kaplan, A.V., Lefèvre, T., Grube, E., Serruys, P.W., 2008. Tryton I, First-In-Man (FIM) study: six month clinical and angiographic outcome, analysis with new quantitative coronary angiography dedicated for bifurcation lesions. EuroIntervention 3, 546–552. http://dx.doi.org/10.4244/EIJV3I5A99.
Pagiatakis, C., Tardif, J.-C., L'Allier, P.L., Mongrain, R., 2015. A numerical investigation of the functionality of coronary bifurcation lesions with respect to lesion configuration and stenosis severity. J. Biomech. 48, 3103–3111. http://dx.doi.org/10.1016/j.jbiomech.2015.07.018.
Peng, C., Wang, X., Xian, Z., Liu, X., Huang, W., Xu, P., Wang, J., 2016. The impact of the geometric characteristics on the hemodynamics in the stenotic coronary artery. PLoS ONE 11, e0157490. http://dx.doi.org/10.1371/journal.pone.0157490.
Pietrabissa, R., Mantero, S., Marotta, T., Menicanti, L., 1996. A lumped parameter model to evaluate the fluid dynamics of different coronary bypasses. Med. Eng. Phys. 18, 477–484.
Pinto, S.I.S., Campos, J.B.L.M., 2016. Numerical study of wall shear stress-based descriptors in the human left coronary artery. Comput. Methods Biomech. Biomed. Eng. 1–13. http://dx.doi.org/10.1080/10255842.2016.1149575.
Pivkin, I.V., Richardson, P.D., Laidlaw, D.H., Karniadakis, G.E., 2005. Combined effects of pulsatile flow and dynamic curvature on wall shear stress in a coronary artery bifurcation model. J. Biomech. 38, 1283–1290. http://dx.doi.org/10.1016/j.jbiomech.2004.06.015.
Prosi, M., Perktold, K., Ding, Z., Friedman, M.H., 2004. Influence of curvature dynamics on pulsatile coronary artery flow in a realistic bifurcation model. J. Biomech. 37, 1767–1775. http://dx.doi.org/10.1016/j.jbiomech.2004.01.021.
Stonebridge, P.A., Buckley, C., Thompson, A., Dick, J., Hunter, G., Chudek, J.A., Houston, J.G., Belch, J.J.F., 2004. Non spiral and spiral (helical) flow patterns in stenoses. In vitro observations using spin and gradient echo magnetic resonance imaging (MRI) and computational fluid dynamic modeling. Int. Angiol. 23, 276–283.
Theodorakakos, A., Gavaises, M., Andriotis, A., Zifan, A., Liatsis, P., Pantos, I., Efstathopoulos, E.P., Katritsis, D., 2008. Simulation of cardiac motion on non-Newtonian, pulsating flow development in the human left anterior descending coronary artery. Phys. Med. Biol. 53, 4875–4892. http://dx.doi.org/10.1088/0031-9155/53/18/002.
van der Giessen, A.G., Groen, H.C., Doriot, P.-A., de Feyter, P.J., van der Steen, A.F.W., van de Vosse, F.N., Wentzel, J.J., Gijsen, F.J.H., 2011. The influence of boundary conditions on wall shear stress distribution in patients specific coronary trees. J. Biomech. 44, 1089–1095. http://dx.doi.org/10.1016/j.jbiomech.2011.01.036.
Van Langenhove, G., Wentzel, J.J., Krams, R., Slager, C.J., Hamburger, J.N., Serruys, P.W., 2000. Helical velocity patterns in a human coronary artery: a three-dimensional computational fluid dynamic reconstruction showing the relation with local wall thickness. Circulation 102, E22–E24. http://dx.doi.org/10.1161/01.CIR.102.3.e22.
Vorobtsova, N., Chiastra, C., Stremler, M.A., Sane, D.C., Migliavacca, F., Vlachos, P., 2016. Effects of vessel tortuosity on coronary hemodynamics: an idealized and patient-specific computational study. Ann. Biomed. Eng. 44, 2228–2239. http://dx.doi.org/10.1007/s10439-015-1492-3.
Wentzel, J.J., Chatzizisis, Y.S., Gijsen, F.J.H., Giannoglou, G.D., Feldman, C.L., Stone, P.H., 2012. Endothelial shear stress in the evolution of coronary atherosclerotic plaque and vascular remodelling: current understanding and remaining questions. Cardiovasc. Res. 96, 234–243. http://dx.doi.org/10.1093/cvr/cvs217.
Zeng, D., Ding, Z., Friedman, M.H., Ethier, C.R., 2003. Effects of cardiac motion on right coronary artery hemodynamics. Ann. Biomed. Eng. 31, 420–429.
Zhang, D., Dou, K., 2015. Coronary bifurcation intervention: what role do bifurcation angles play? J. Interv. Cardiol. 28, 236–248. http://dx.doi.org/10.1111/joic.12203.